Solar Energy Materials & Solar Cells 230 (2021) 111286

Contents lists available at ScienceDirect

Solar Energy Materials and Solar Cells

journal homepage: www.elsevier.com/locate/solmat

A facile approach to achieve subambient radiative cooling through aluminum foils and polyethylene bubble wrap

Yanpei Tian [a], Xiaojie Liu [a], Fangqi Chen [a], Yi Zheng [a,b,*]

[a] Department of Mechanical and Industrial Engineering, Northeastern University, Boston, MA 02115, USA
[b] Department of Electrical and Computer Engineering, Northeastern University, Boston, MA 02115, USA

ARTICLE INFO

Keywords:
Subambient radiative cooling
Polyethylene bubble wrap
Cost-effective
Infrared-transparent
Thermal-insulating

ABSTRACT

Subambient radiative cooling is an emerging passive cooling strategy that simultaneously reflects the incident solar irradiance to depress the heat gain and radiates heat from objects to enhance the heat loss without any electricity consumption from compressor-based air-conditioning. Although numerous efforts have been dedicated to developing materials, such as complicated photonic crystals and metamaterials or expensive polymer composites with both high solar reflectance and infrared emittance, the gap still exists between efficient radiative cooling performance and an affordable radiative cooling device. Here, a facile, low-cost, and home-built approach to achieve efficient subambient radiative cooling, which employs commercially available materials of the polyethylene (PE) bubble wrap and aluminum foils, is reported for scalable industrial and domestic applications. The aluminum foils are infrared-reflective and sunlight-opaque, acting as a solar shield and infrared waveguide, which can both block the solar irradiation and guide infrared thermal radiation to the cold outer space. PE thin film is infrared-transparent with a high mid-infrared transmittance that allows mid-infrared thermal radiation to pass through. It is thermally insulating with a low thermal conductivity of 0.038 W/m · K after being fabricated into air-filled bubbles to minimize parasitic non-radiative heat transfer. An average subambient temperature reduction of 4.0°C has been achieved during the noontime in summer. These commercially available materials make this design a practical technique for people to realize an affordable and comfortable interior environment during the summer in a cost-effective manner without any professional constructions. The nature of low-cost, home-built, and easily integrated into buildings renders it attractive for everyone, especially for those in developing regions.

1. Introduction

Energy shortage is one of the major issues for humans in the 21st century [1]. A huge amount of greenhouse gas emissions severely accelerate global climate change and frequent extreme weather [2,3]. Among those, space heating and cooling contribute to ~ 15% of the primary energy usage in the United States and ~ 70% of the electricity consumption in some topical regions [4,5]. Reducing the energy demand for thermal regulation of the indoor environment has a substantial impact on global energy consumption and climate change. Therefore, a passive, affordable, scalable, and efficient cooling technique that cools down an object without any energy input and CO_2 emissions is urgently demanded by the green-energy society. The atmospheric windows from 8 μm to 13 μm and 16 μm to 20 μm, which is highly transparent to mid-infrared thermal radiation, corresponds to the natural infrared emission of terrestrial objects (20 – 40 °C) from 5 μm to 20 μm. The first atmospheric window contributes mainly to the radiative cooling effect when an object's temperature is around 300 K, while the second atmospheric window is a supplement to the main atmospheric window and it can help to enhance the radiative cooling performance when an object's temperature drops and its peak thermal radiation shifts right to longer wavelengths according to the Wien's displacement law. The atmospheric window builds a "bridge" through which terrestrial objects can radiate heat as infrared radiation to the outer space as a cold sink (~ 3 K) [6–8].

Radiative cooling is theoretically potential to cool objects down up to 60 °C below ambient temperature by employing a highly selective thermal emitter spectrum matched to the atmospheric window and using the vacuum enclosure to minimize parasitic heat losses [15]. Different approaches have been investigated to achieve subambient radiative cooling. Approach I: A radiative cooler can achieve a subambient temperature reduction by modifying its surface radiative properties to have a high solar reflectance to minimize solar heating and high

* Corresponding author at: Department of Mechanical and Industrial Engineering, Northeastern University, Boston, MA 02115, USA.
E-mail address: y.zheng@northeastern.edu (Y. Zheng).

https://doi.org/10.1016/j.solmat.2021.111286
Received 12 March 2021; Received in revised form 12 June 2021; Accepted 13 July 2021
Available online 23 July 2021
0927-0248/

Table 1
Comparison of different radiative cooling approach.

Materials[a]		Fabrication method[b]	Temperature drop (°C)	Cooling power (W/m^2)
Approach I	PVDF-HFP [9]	Phase inversion	6	96
	TPX+SiO_2 [10]	Roll-to-Roll	10.6	100
	PVDF/SiO_2 [11]	Electrospinning	4	80
	Bleached wood [6]	Bleached + hot press	6	103
Approach II	PE aerogel [12]	TIPS[2]	13	96
	Nanoporous PE [13]	Thermal Extrusion	2.3	–
	PE aerogel [14]	TIPS	6	70
Our approach	PE bubble wrap + aluminum foils	Home-built	4	–

[a]PVDF-HFP: Poly(vinylidene fluoride-co-hexafluoropropylene); TPX: Polymethylpentene; SiO_2: Silicon dioxide; PVDF: Polyvinylidene fluoride.
[b]TIPS: Thermally induced phase separation.

thermal emittance over the atmospheric window to enhance radiative cooling (Fig. 1(a) and (b)). Approach II: When a radiative cooler has a surface with high solar reflectance and selective infrared transmittance over the atmospheric window. The excellent thermal insulation can significantly reduce the parasitic heat gain from warm ambient via thermal conduction and convection (Fig. 1(c) and (d)).

Remarkable progress has been made recently to achieve subambient radiative cooling by following either the same mechanism of approach I or approach II. The spectrum manipulations for approach I were realized by the design of 1-D [7,15], 2-D [16,17], and 3-D [18] photonic structures, photonic metamaterials [6,8,9], and pigmented paints [19]. Several infrared-transparent materials like polyethylene (PE) thin films [1,12,13,20], Zinc selenide [21], Germanium [22], Cadmium sulfide [23] as infrared-transparent cover are validated for radiative cooling. Porous PE thin films or sheets that are infrared-transparent materials with high solar reflectance and low thermal conductivity like approach II were developed to achieve subambient cooling effects [12,13] by enhanced backscattering of the sunlight. Although subambient radiative cooling effects have been achieved in the works abovementioned, it is still challenging for scalable deployment resulting from expensive and complicated fabrication methods, high-cost materials, and time-consuming integration into building roofs like inflexible materials. These high requirements also hinder the implementation for wider regions, especially for those less-developed countries with weak industries. Hence, a strategy that relies on only commercially available materials, cost-effective, and easy-deployed will be more promising for both industrial and residential applications.

PE bubble wraps are often formed from low-density polyethylene (LDPE) thin film with regularly spaced and protruding air-filled hemispherical bubbles and are used to provide cushioning for fragile or sensitive objects in our daily lives. Encapsulated air within bubbles gives bubble wraps a low thermal conductivity of 0.038 W/m K, which is less than one-tenth of the thermal conductivity of PE thin film (0.4 W/m K). PE bubble wraps also inherit the high infrared transmittance of PE thin films. It can synchronously minimize the parasitic heat gain and ensure that the infrared thermal radiation from objects passes through as a thermal insulating cover. Aluminum foil is a common household item that is often used for packaging, cooking, and electromagnetic shielding. It can reflect almost 100% mid-infrared thermal radiation with a wavelength over 1 μm and is a perfect infrared waveguide material. By taking advantage of the good thermal insulating effects and high transparency to mid-infrared light of PE bubble wraps, as well as the high reflectance of aluminum foil, subambient radiative cooling can be achieved. Materials for outdoor radiative cooling undergo harsh environment exposure (UV, dust, and precipitations) can severely reduce its solar reflectance. Meanwhile, considering that the theoretical limit of radiative cooling power is ~ 170 W/m^2 [24] and the solar intensity of global horizontal irradiance is around 1,000 W/m^2, even a 5% reductions of solar reflectance, as described in the approach I and approach II, will undermine 30% of its ideal performance. Too many efforts have been allocated to develop materials with high solar reflectance over the solar wavelengths including UV, visible, and near-infrared wavelengths, but high reflectance in visible wavelengths restricts their application in real-life situations, meaning that white colors under sunlight might harm human eyes and monochromatic coating for buildings or other objects will deteriorate artistic designs [25]. Fortunately, 79.4% of the world's population is concentrated within 20–60° of north latitude area and incident angles of the sunlight vary with season changes. Furthermore, the slope of roofs leaves more space for us to design a simple solar shield to block all the solar irradiance without the sacrifice of aesthetic designs using materials like aluminum foils or wood boards. Common building materials like wood, brick, glass, and concrete have relatively high emittance (~ 0.85), and their emittance increase above 0.9 after painted into different colors in the mid-infrared region (Fig. S1 and S2). As shown in Fig. 1(e), we employ the aluminum foil-covered wood board as a solar shield and PE bubble wraps as a thermal barrier to reduce the parasitic heat gain from the ambient without blocking the radiative heat transfer between the cold outer space and objects beneath bubble wraps. The comparison between our approach and published works is listed in Table 1.

Here, we theoretically and experimentally demonstrate effective subambient radiative cooling by employing PE bubble wraps, thermally insulating and infrared-transparent materials, and aluminum foils that are highly reflective to mid-infrared thermal radiation. The potential of the radiative cooling power for the approach I, II, and our proposed approach as a function of temperature under different non-radiative heat transfer coefficients are theoretically investigated. We also experimentally determined the optical and thermal properties of the PE bubble wraps and aluminum foils. The temperature of the back-insulated thin-film heater covered by PE bubble wraps shows 2.6 °C and 1.2 °C below the cotton wrap covered and the polyester covered under the same heating power density, respectively. Subambient radiative cooling performance is validated in the laboratory environment with liquid nitrogen (N_2) as a cold source. The outdoor experiment validates an average subambient temperature reduction of 4.0 °C during the noontime in summer. These demonstrations show the potential of the proposed approach, consisting of commercial and low-cost materials, for facial, easily-deployed, affordable, and efficient radiative cooling, which is especially achievable for less-developed countries.

2. Materials and methods

2.1. Materials

The PE bubble wraps, balsa wood, glass sheet, concrete, brick, thin-film heater, K-type thermocouples, ceramic tile, and wind shield were purchased from Amazon. The bubble wrap has a bubble diameter of 9 mm and the centers of these bubbles are arranged at an equal distance of 11 mm. Copper sheets and PS foam were provided by McMaster-Carr and the aerogel blanket was from Aerogel Technologies, LLC.

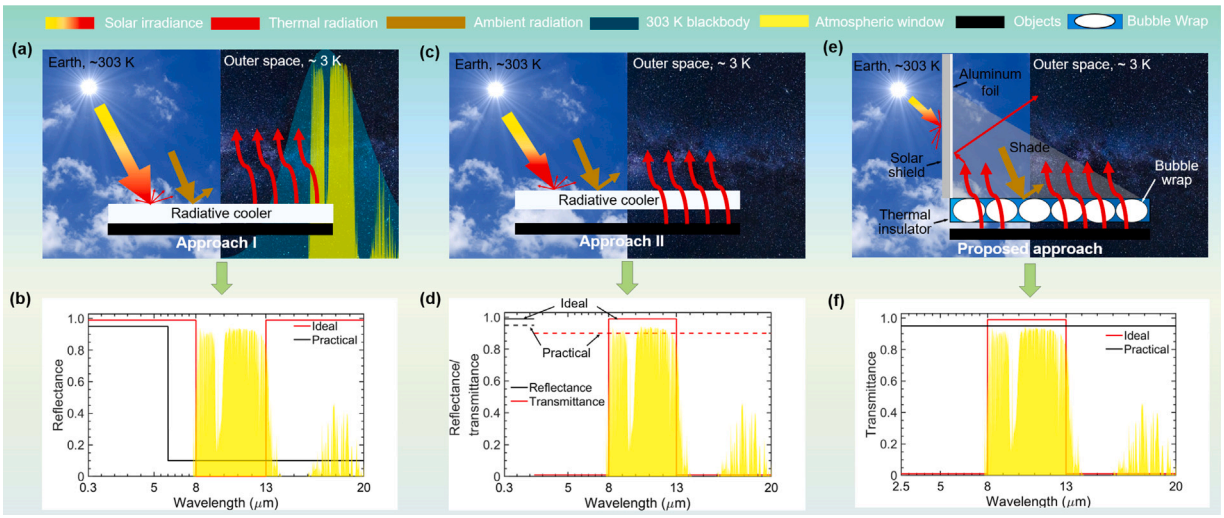

Fig. 1. Schematic of different approaches for radiative cooling. (a) The approach I for subambient radiative cooling: A radiative cooler facing outer space with high solar reflectance to reduce maximally solar heating and high thermal emittance to radiate efficiently extra heat to the cold outer space. (b) The reflectance spectra of ideal and practical thermal emitter for the approach I displaying with the atmospheric transmittance spectrum. Ideal: the radiative cooler has unity solar absorptance and unity thermal emittance from 8 μm to 13 μm and 16 μm to 20 μm. Practical: the radiative cooler for real-life applications with solar reflectance less than unity and non-selective thermal emittance less than unity beyond 6 μm. (c) Approach II for subambient radiative cooling: optically selective and thermally insulating layer sitting on top of objects. The radiative cooler is thermally insulated that can depress simultaneously heat gain from solar irradiance and parasitic heating effects from the ambient convection and radiation. It is infrared-transparent to infrared thermal radiation for objects radiating heat to outer space. (d) The reflectance spectra of ideal and practical optically selective and thermally insulating layer for the approach II. Ideal: the radiative cooler has unity reflectance over the solar wavelength from 0.3 μm to 2.5 μm and unity transmittance over the atmospheric window from 8 μm to 13 μm and 16 μm to 20 μm. Practical: the practical radiative cooler displays solar reflectance less than unity and a broadband thermal emittance less than 1 from 2.5 μm to 20 μm. (e) Our proposed approach for subambient radiative cooling where the solar shield blocks all the incident solar irradiation and PE bubble wraps act as a thermal insulating layer to block ambient convective heat transfer. The PE bubble warp is also highly infrared transparent to ensure the radiative heat transport from objects to outer space. The back of the solar shield is covered by infrared-reflective aluminum foils (Fig. S3), acting as a waveguide, to reflect the emitted thermal radiation from objects to the other half of the sky. (f) The transmittance spectra of ideal and practical for our proposed approach. Ideal: the radiative cooler has selective transmittance only over these two atmospheric windows. Practical: the practical radiative cooler with a transmittance (~ 0.9) over the whole mid-infrared region (2.5 μm–20 μm).

2.2. Methods

2.2.1. Indoor radiative cooling experiments

The liquid N_2 was filled into a plastic tank with a bottom-insulated by 1 inch thick PS foam sheet and it serves as a cold source to receive the thermal radiation from objects that needed to be cooled down. The distance between the top chamber and the level of the liquid N_2 was about 0.7 m. Temperatures of the chamber, the back of samples, and the ambient were recorded by K-type thermocouples connected to the PICO thermocouple data logger at a frequency of 1 Hz.

2.2.2. Outdoor radiative cooling experiments

The temperature variations of samples were monitored by using the K-type thermocouples connected to the National Instruments (NI) PXI-6289 multifunction I/O module at a frequency of 1 Hz. The solar shield was made of a 1-inch thick wood sheet and was covered by 16 μm thick aluminum foils as the infrared reflector. The thermocouple for recording ambient temperature was shielded into a wind shield to make the accuracy of the measurement. The weather station recorded the solar intensity, relative humidity, and wind speed.

2.2.3. Materials characterizations

Thermal conductivities of samples were measured by the isotropic standard module of TPS 2500s. The infrared hemispherical reflectance spectra (2.5 μm–20 μm) were characterized by Jasco FTIR 6600 equipped with a PIKE upward gold integrating sphere. Angle-dependent infrared transmittance spectra were measured by Jasco FTIR 6600 with Harrick variable angle transmission accessory with an angle increment of 15° from 0° to 80°. Infrared images were taken using FLIT A655C thermal camera with 25° lens at a resolution of 640 × 480. The material characterizations are conducted at around 21 °C.

3. Results and discussions

3.1. Theoretical model to evaluate the potential of different approaches for radiative cooling

To accurately evaluate the performance of different approaches for radiative cooling, a theoretical model was developed. Here, we assume that there is no heat loss from the back and side of the object. The energy balance of the object is:

$$P_{net}^{cooling} = P_{rad}\left(T_{obj}\right) - P_{sun}\left(T_{obj}\right) - P_{nr}\left(T_{air}, T_{obj}\right) - P_{amb}\left(T_{air}\right) \quad (1)$$

We take the radiative cooling power to be P_{rad} and the temperature of objects to be T_{obj}. P_{sun} represents the absorbed solar heating power. P_{nr} is the non-radiative power between the objects and the ambient air, P_{amb} is defined to be the incident thermal radiative power from the ambient thermal radiation. T_{air} stands for the ambient temperature. $P_{net}^{cooling}$ denotes the radiation power density of the object:

$$P_{rad}\left(T_{obj}\right) = \int_0^{\infty} \mathrm{d}\lambda I_{BB}\left(T_{obj}, \lambda\right) \epsilon\left(\lambda, \theta, \phi, T_{obj}\right) \quad (2)$$

where, $I_{BB}(T_{black}, \lambda) = 2hc^2\lambda^{-5} \exp(hc/\lambda k_B T_{obj} - 1)^{-1}$ defines the spectral radiance of blackbody. Here, h is the Planck's constant, c is the light speed, λ is the wavelength, and k_B is the Boltzmann constant. $\epsilon(\lambda, \theta, \phi, T_{obj}) = \frac{1}{\pi}\int_0^{2\pi} \mathrm{d}\phi \int_0^{\pi/2} \epsilon_\lambda \cos\theta \sin\theta \mathrm{d}\theta$ is the temperature-dependent emittance of the object [26]. θ and ϕ are the azimuthal and latitudinal angles of the sun irradiance.

$$P_{sun}(T_{obj}) = I_{sun}(t) \cdot \epsilon(T_{obj}) \quad (3)$$

where I_{sun} means the solar intensity at AM 1.5. $\epsilon(T_{obj})$ represents the wavelength- and temperature-dependent absorbance of the object.

The non-radiative heat transfer between the object and the ambient air is expressed as:

$$P_{nr}(T_{air}, T_{obj}) = h_{nr}(T_{air} - T_{obj}) \quad (4)$$

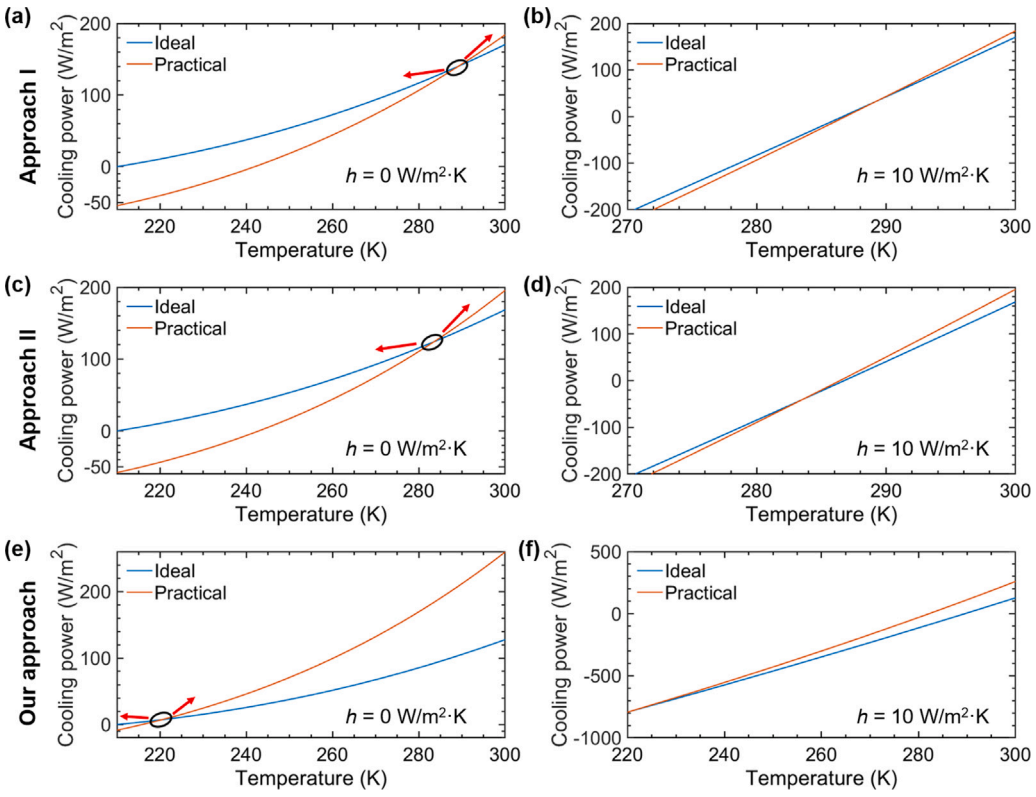

Fig. 2. Performance of different radiative cooling approaches. The simulated net radiative cooling power of the ideal and practical for the approach I as a function of the temperature of objects with different non-radiative heat transfer coefficients (a) h = 0 and (b) h = 10 W/m^2 K under AM 1.5 irradiance, while (a) and (b) represents approach I. (c) and (d) are for approach II, and (e) and (f) display our proposed approach. The ambient temperature is set to be 300 K for these simulations. The objects below the radiative cooler in approach II and our proposed approach are considered to be blackbody over the wavelength of interest from 0.3 μm to 20 μm.

where, h_{nr} is the non-radiative heat transfer coefficient. The absorbed power density from the surrounding atmosphere, $P_{amb}(T_{air})$ is:

$$P_{amb}(T_{air}) = \int_0^\infty \mathrm{d}\lambda I_{BB}(T_{air}, \lambda)\epsilon(\lambda,\theta,\phi,T_{obj})\epsilon_{amb}(\lambda,\theta,\phi) \tau(\lambda,\theta,\phi) \quad (5)$$

The emittance of the ambient, $\epsilon_{amb}(\lambda,\theta,\phi)$, is given by $1-\tau_{amb}(\lambda,\theta,\phi)$. Here $\tau_{amb}(\lambda,\theta,\phi)$ is the transmittance value of atmosphere obtained from MODTRAN 4 [27]. $\tau_{amb}(\lambda,\theta,\phi)$ means the transmittance of the thermal insulator in approach II and our proposed approach. The control volume for the thermal analysis only includes the radiative cooler.

As shown in Fig. 1(b) for the approach I, the reflectance spectrum of the radiative cooler for the ideal has a unity solar absorbance to reduce the solar heating, unity thermal emittance over the atmospheric window, and zero emittance otherwise, and this is ideal for the subambient radiative cooling performance. While the reflectance spectrum of practical shows a solar reflectance less than 1 and thermal emittance of about 0.9 at a broad spectral region beyond 6.0 μm, which is closer to the practical situation. The net cooling power density as a function of object temperature without and with non-radiative parasitic influence are shown in Fig. 2(a) and (b), respectively. Fig. 2A shows that practical, emitting thermal radiation outside the atmospheric window to the ambient air, has a larger cooling power density than the ideal for higher temperatures above 273 K. While the absorbed radiative heating power from the ambient of practical is larger than that of ideal, the power radiated outward to the ambient increases by a larger amount. Therefore, expanding the spectral range of unity emittance outside the atmospheric window can be beneficial to increase the net cooling power density under such circumstances that the temperature of cooling objects is higher than ambient temperature. The ideal is preferred when one aims to achieve a substantially subambient temperature, while practical is better for maximally harvesting the coldness of the outer space but with a relatively higher cooling temperature demand. For ideal, high vacuum or thermal insulation is required to minimize parasitic conduction and convection heating gain [28]. If parasitic non-radiative heating effects are present, as shown in Fig. 2(b) (h = 10 W/m^2 K), expanding the spectral wavelengths with unity emittance benefits to attain a higher net cooling power density. Similar trends also exhibit in approach II, the narrowband transmittance spectra of the radiative cooler do not always have an advantage over the broadband radiative cooler. As the temperature of the radiative cooler increases, the high transmittance outside the atmospheric window can also be favorable to reach a higher net cooling power density, as shown in Fig. 2(c) and (d). The difference between approach II and our proposed approach is whether the radiative cooler needs to be highly reflective of solar wavelengths. We use the solar shield to eliminate the need of designing an "ultra-white" surface to reflect the sunlight and use the aluminum foil to guide the out-emitting infrared thermal radiation to the sky. This leaves much more space for low-cost and commercially available materials, aesthetic designs, and easy deployment.

3.2. Optothermal characterizations of PE bubble wraps

PE with a chemical formula $(C_2H_4)_n$ (the bottom inset of Fig. 3(a)) is the most common thermoplastic with high annual production in our daily life and can be classified as LDPE, MDPE, and HDPE (LD: Low-density; MD: Medium-density; HD: High-density) according to their density. The LDPE PE thin film with protruding air-filled bubbles sandwiched between two PE thin films are called bubble wraps (Fig. 1(a)). The mechanical strength of bubble wraps is enough to fulfill the requirement of engineering applications (the top inset of Fig. 3(a)) and its flexibility renders it to match various shapes of the building roofs. Air is a good thermal insulation material (0.026 W/m^2 K at 20 °C) and the

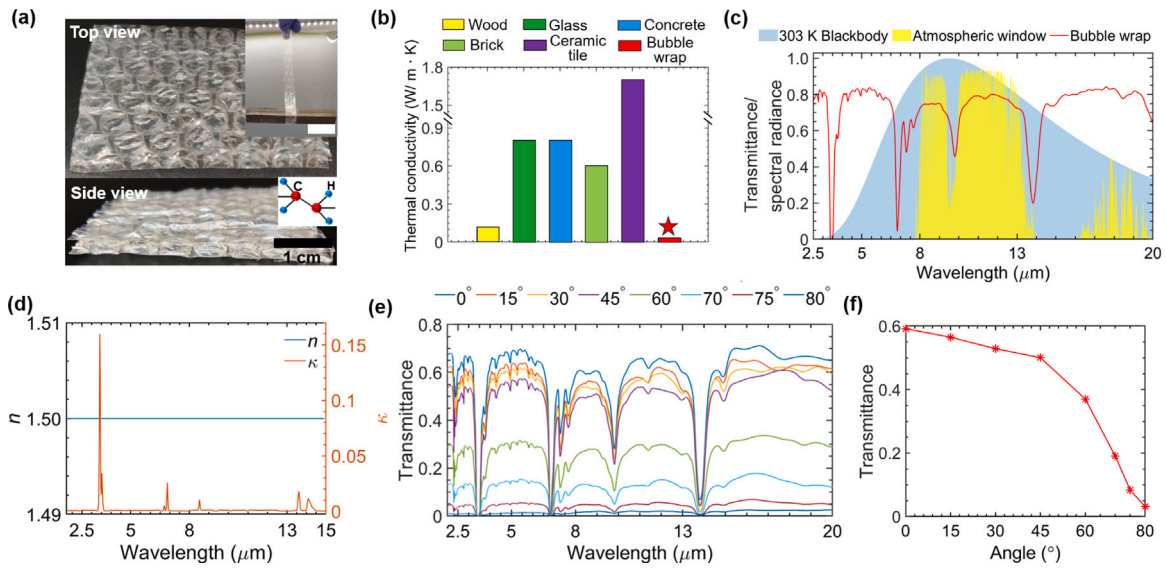

Fig. 3. Optical and thermal characterization of PE bubble wraps. (a) Photographs of a 5 cm × 5 cm × 0.38 cm thick PE bubble wrap sample. The thickness of the PE thin film that is used to fabricate the bubble wrap is 40 μm. The top inset shows the good mechanical strength of PE bubble wrap, and its scale bar is 2 cm. The bottom inset displays the chemical formula of PE. (b) Comparison of the PE bubble wraps with general building materials. (c) Hemispherical transmittance and reflectance of a 0.38 cm PE bubble wrap sample displaying with the atmospheric transmittance and the normalized 303 K blackbody radiation. (d) Complex refractive indices (n, refractive index, and κ, extinction coefficient) of the PE for the infrared wavelengths. (e) The transmittance spectra of the PE bubble warp at various incident angles. (f) The average transmittance of the PE bubble wraps over the atmospheric transparent window as a function of incident angles.

encapsulated air inside bubbles makes PE bubble wrap a good thermal insulating material (0.038 W/m^2 K at ~ 21 °C), significantly lower than those common building materials (Fig. 3(b)). Air is highly transparent to infrared lights from 8 μm to 13 μm and PE, consisting of only aliphatic C–C and C–H bonds with narrow absorption bands at wavelengths of 3.4, 6.8, 9.8, and 13.7 μm. Infrared transparent air and PE thin films ensure that PE bubble wraps show high hemispherical transmittance over the entire atmospheric window (Fig. 3(c)). This is also reflected in the spectral complex refractive indices. The extinction coefficient, κ, exhibits ultra-narrow absorption peaks at 3.4, 6.8, 13.7, and 14.2 μm and negligible extinction coefficient otherwise (Fig. 3(d)). The high transmittance of PE bubble wraps retains over a large incident angle of 0–45° (Fig. 3(e) and Fig. S4), and the average transmittance over the atmospheric window decreases slightly when the incident angle is less than 45° (Fig. 3(f)), which guarantees that the emitted thermal emission from objects can efficiently radiate to the outer space.

3.3. Experimental validations of the high infrared transparency for PE bubble wraps

We experimentally demonstrate the high transparency of PE bubble wrap with a device as shown in Fig. 4(a). Those four open chambers are either open to the air or covered by cotton wrap, polyester textile, or PE bubble wraps. The cotton wraps and polyester textile are highly opaque to infrared wavelengths (Fig. 4(b)), and they block the channel of the radiative heat transfer between the thin-film heater and the ambient. A triangular copper sheet is used to show the infrared transmittance by use of infrared imaging (Fig. 4(c)). Whereas the bare copper and bubble wrap clearly show the triangular shape, cotton or polyester does not show the metallic pattern. Such difference in infrared transmittance is because the infrared absorption wavelengths, resulting from the vibrations of the chemical bonds of cotton and polyester like C–O stretching (7.7 μm – 10 μm), aromatic C–H bending (7.8 μm –14.5 μm) [1], overlap with the atmospheric window. The emitted infrared radiation is blocked by the cotton and polyester and the thermal camera can only capture the re-emitted thermal wavelengths from the top surface of cotton and polyester. The polyester textile has the highest thermal conductivity, but they are at the same order of magnitude (Fig. 4(d)). Under various heating power intensities of these four thin-film heaters, their surfaces on the back show different stagnation temperatures as shown in Fig. 4(e). The cotton wraps have the highest stagnation temperature because of their highest opaqueness and lowest thermal conductivity (Fig. 4(b) and (d)) compared with polyester textile and bubble wraps at the same thickness. PE bubble wraps show the lowest temperature due to their high transparency even though their thermal conductivity is relatively lower than the polyester.

3.4. Indoor radiative cooling experiment

A schematic of the indoor radiative cooling experimental setup is shown in Fig. 5(a). The bottom tank is filled with liquid N_2 (~ 77 K) as a cold source to simulate outer space. The emittance of the plastic container approaches unity (Fig. S5) and can be regarded as a cold blackbody to absorb all thermal radiation. The examined samples are commonly used building materials, e.g., wood and concrete, which show high infrared emittance to release its heat through radiative heat transfer (Fig. 5(b)). The wood and the concrete emitter is sealed in a PS foam container fixed at the top with PE bubble wraps covered, facing down to the liquid N_2 tank, and three thermocouples are placed at different locations to show the cooling performance, as indicated in Fig. 5(a). The stabilized temperature of concrete is 13.95 °C below the ambient, while the wood shows a stagnation temperature that is 12.33 °C below the ambient. It is because that the concrete has a relatively higher infrared emittance (0.81) than wood (0.79) and its thermal conductivity (0.8 W/m K) is much larger than wood (0.12 W/m K perpendicular to the grain). The chamber temperature drop results from the cooling effects of wood and concrete.

3.5. Outdoor radiative cooling experiment

To evaluate the radiative cooling performance in real-life application, we performed outdoor tests at Northeastern University, Boston, from 10:10 AM to 12:00 AM on June 16, 2020, under a clear sky, a wind speed of ~ 3 km/h, and relative humidity (RH) of ~ 60% as shown in Fig. S7(a). Three different samples: wood, concrete, and black painted copper sheet with the same thickness were placed on top of 6 mm aerogel blankets in sealed PS foam containers and the top of these chambers were covered by PE bubble wraps. All of these

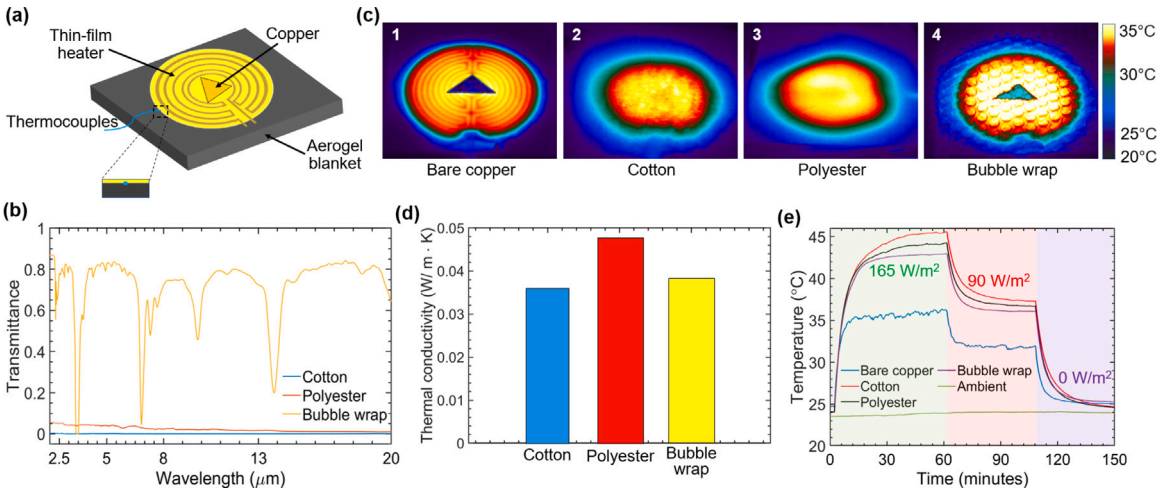

Fig. 4. Radiative thermal measurement of PE bubble wraps. (a) A schematic of indoor radiative thermal measurement of the PE bubble wraps. The polyimide thin-film heater with a diameter of 10 cm sitting on top of a 6 mm thick aerogel blanket generates constant heating power, serving as a heat source. The temperature variations of the back of the thin film heater are recorded by a K-type thermocouple. A 0.5 mm thick copper sheet in a shape of an equilateral triangle is placed on top of the center of the thin-film heater. All the elements listed above are put in a chamber of polystyrene (PS) foam with thermal conductivity of 0.035 W/m K. The windows of these four chambers are either open to the ambient or covered by a cotton wrap, polyester textile, and PE bubble wraps. (b) The infrared hemispherical transmittance spectra of the cotton wrap, the polyester textile, and the PE bubble wraps. The PE bubble wraps are infrared-transparent, while the cotton wrap and polyester textile are infrared-opaque. (c) Infrared thermal images of the bare copper sheet and the other three samples covered by the cotton wrap, the polyester textile, and the PE bubble wraps, respectively. Only the PE bubble wraps can reveal the triangular metallic pattern resulting from its infrared transparency. (d) Thermal conductivity of the cotton wrap, the polyester textile, and the PE bubble wraps. (e) Temperature variations of the back of the thin film heater under different heating power intensities. The one with the PE bubble wraps covered has the lowest temperature rise due to its infrared transparency. The first and second stable temperature regions are heated under 165 W/m^2 and 90 W/m^2, respectively.

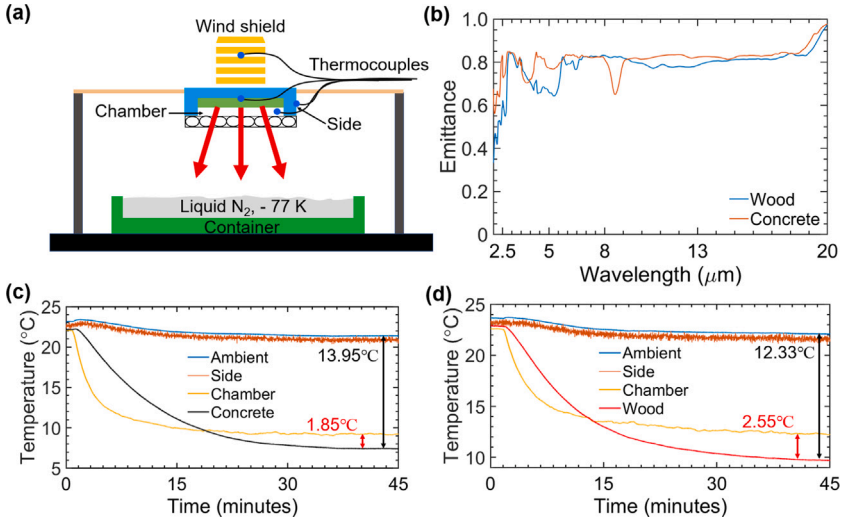

Fig. 5. Indoor radiative cooling performance of the PE bubble wraps. (a) A schematic diagram of the indoor radiative cooling experimental setup. A plastic container with liquid N_2 at ~ 77 K can be regarded as a cold source. Temperature variations are monitored by K-type thermocouples. The thermocouple for recording the ambient temperature is inserted into a wind shield box. (b) The hemispherical emittance spectra of 1.5 mm thick wood and concrete samples (ϵ (emittance) = 1 – R (reflectance) when the object is opaque). Temperature curves of the ambient, chamber, (c) concrete, and (d) wood. The side temperature is around 0.5 °C below the ambient.

containers are in a modified cooler box (Fig. 6(a) and (b)). A wood board with aluminum foils covered serving as both a solar shield to block all the incident solar irradiance and a waveguide to direct the emitted thermal radiation to the sky. We can see that the temperature of copper with black paint increases up to 90 °C without the solar shield before 10:45 AM due to its high solar reflectance and high thermal conductivity (385 W/m K), while the wood approaches to only 46 °C because of its high solar reflectance in the near-infrared region (0.8 μm to 2.5 μm) and low thermal conductivity (0.12 W/m K) (Fig. 3(b) and Fig. S6). After the solar irradiation was blocked by the solar shield, temperatures of wood, concrete, copper drop and are stable after 11:30 AM, the inset of Fig. 6(c) shows that the temperature reductions of the wood and concrete samples are 4.0 °C and 3.6 °C below the ambient, respectively even in weather of high humidity and wind speed (Fig. S7(a)). Our proposed design can be adjusted to adapt different roof styles (Fig. 6(d)). The subambient radiative cooling effects can alleviate the energy consumption of air conditioning in the summer and the easy-deployed and cost-effective features will be of importance to less-developed countries. To further demonstrate the radiative cooling effect for real-world applications, we fabricated two mini houses with the 2 mm thick wood board and run the outdoor experiment at Northeastern University, Boston, MA from 11:30 to 13:00 on June 10, 2021 (Fig. 6(e) and Fig. S8). The left mini house is equipped with a solar shield, aluminum foil as an infrared reflector, and PE bubble wrap on its roof. The K-type thermocouple is placed in the middle of the mini house to monitor the temperature variations of their inner environment. The right house is a reference group without the proposed radiative cooling approach. The mini houses are placed on a 25 mm thick PS foam board

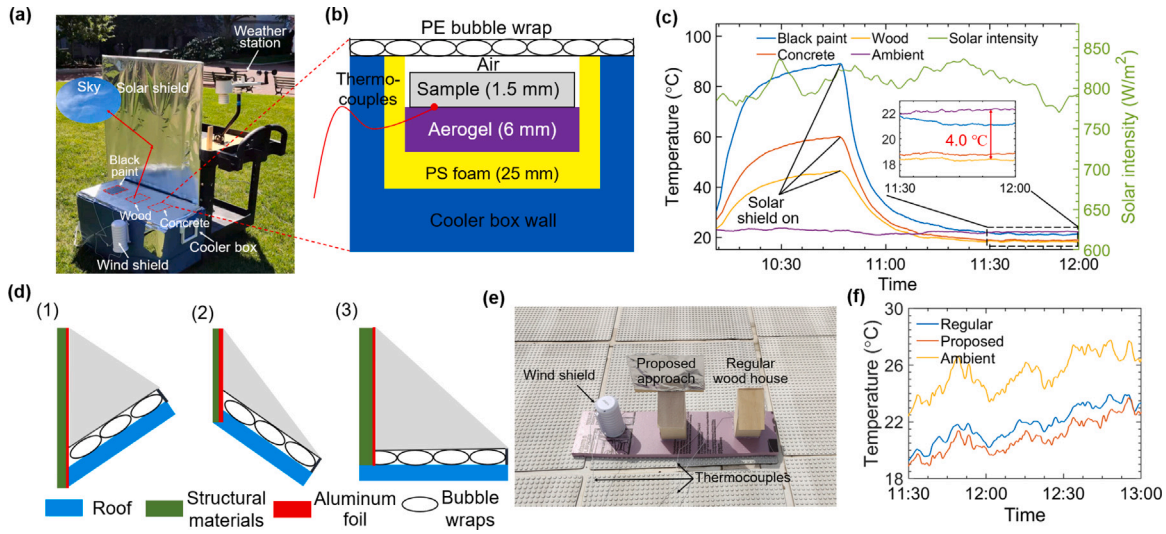

Fig. 6. Outdoor radiative cooling measurement. (a) A photograph of the outdoor radiative cooling experiment. Three 1.5 mm thick samples of black painted copper sheet, wood, and concrete are placed on top of a 6 mm thick aerogel blanket. The thermocouple records the back temperature of these samples. The surface of the solar shield is covered by 16 μm thick aluminum foils as the infrared reflector that reflects the emitted thermal energy through the PE bubble wraps to the sky. (b) A schematic of the experimental setup inside the cooler box. (c) Temperature variations of these three samples and the solar intensity during the experimental period. Inset shows the details of the temperature curves from 11:30 AM to 12:00 PM on June 16, 2020, Boston, MA. (d) Schematic illustrations of the PE bubble wrap and aluminum foils enabled radiative cooling structures for large-scale applications. (e) A photograph of wood mini houses for the outdoor radiative cooling experiment. (f) Temperature over time of the mini house modified by the proposed radiative cooling approach and a regular mini house for comparison on June 10, 2021, Boston, MA.

and their bottom are also insulated by the PS foam with the same thickness to minimize the heat conduction between the ground and the inner environment of mini houses. The solar shield is large enough to block the solar irradiance while in use. The size of the solar shield can be adjusted according to the location and the incidence angle of the sun to get a full block of solar irradiation. During the experimental period, the inner temperature of these two mini houses is below the ambient due to the thermal insulation effect from the wood board. The temperature of the mini house with our proposed cooling approach is 1.0 °C on average below that of the regular mini house (Fig. 6(f)). The inner temperature of the mini house with our proposed cooling approach is 4.5 °C below the ambient, resulting from the radiative cooling effect of the PE bubble wrap and thermal insulation effect of the wood board (Fig. 6(f)) even in windy weather (Fig. S7(b)).

4. Conclusions

In summary, we develop a facile, cost-efficient, and efficient passive subambient radiative cooling strategy by employing low-cost, easily deployed, and commercially available materials like aluminum foils and PE bubble wraps. The aluminum foil, which is infrared-reflective and sunlight-opaque, blocks the solar irradiance and guides the thermal emission from objects directly to outer space. The PE bubble wraps, which have low thermal conductivity and high mid-infrared transmittance, can impede parasitic ambient heat load and allow infrared thermal radiation from objects beneath to go through. Our proposed device realizes an average subambient temperature drop of 4.0 °C during the noontime in summer with a remarkable material cost of $2/m^2. The cost-effective, home-built, scalable, and efficient radiative cooling features of our device render it highly competitive compared with other compressor-based cooling techniques and emerging radiative cooling materials. The disruptive design yields the potential to convert passive radiative cooling technology in a broad range of industrial and residential implementations.

CRediT authorship contribution statement

Yanpei Tian: Conceptualization, Methodology, Writing. **Xiaojie Liu:** Writing - review & editing. **Fangqi Chen:** Methodology. **Yi Zheng:** Methodology, Supervision, Writing - review & editing.

Declaration of competing interest

The authors declare that they have no known competing financial interests or personal relationships that could have appeared to influence the work reported in this paper.

Acknowledgment

This project is supported by the National Science Foundation, USA through grant number CBET-1941743.

Appendix A. Supplementary data

Supplementary material related to this article can be found online at https://doi.org/10.1016/j.solmat.2021.111286.

References

[1] P.-C. Hsu, A.Y. Song, P.B. Catrysse, C. Liu, Y. Peng, J. Xie, S. Fan, Y. Cui, Radiative human body cooling by nanoporous polyethylene textile, Science 353 (6303) (2016) 1019–1023.
[2] G.-R. Walther, E. Post, P. Convey, A. Menzel, C. Parmesan, T.J. Beebee, J.-M. Fromentin, O. Hoegh-Guldberg, F. Bairlein, Ecological responses to recent climate change, Nature 416 (6879) (2002) 389–395.
[3] N. Oreskes, The scientific consensus on climate change, Science 306 (5702) (2004) 1686.
[4] S. Chu, A. Majumdar, Opportunities and challenges for a sustainable energy future, Nature 488 (7411) (2012) 294–303.
[5] C. Segar, Renewable augment gas Saudi energy mix, J. IEA 7 (4), 0000.
[6] T. Li, Y. Zhai, S. He, W. Gan, Z. Wei, M. Heidarinejad, D. Dalgo, R. Mi, X. Zhao, J. Song, et al., A radiative cooling structural material, Science 364 (6442) (2019) 760–763.
[7] A.P. Raman, M. Abo Anoma, L. Zhu, E. Rephaeli, S. Fan, Passive radiative cooling below ambient air temperature under direct sunlight, Nature 515 (7528) (2014) 540–544.
[8] Y. Zhai, Y. Ma, S.N. David, D. Zhao, R. Lou, G. Tan, R. Yang, X. Yin, Scalable-manufactured randomized glass-polymer hybrid metamaterial for daytime radiative cooling, Science 355 (6329) (2017) 1062–1066.
[9] J. Mandal, Y. Fu, A.C. Overvig, M. Jia, K. Sun, N.N. Shi, H. Zhou, X. Xiao, N. Yu, Y. Yang, Hierarchically porous polymer coatings for highly efficient passive daytime radiative cooling, Science 362 (6412) (2018) 315–319.
[10] D. Zhao, A. Aili, Y. Zhai, J. Lu, D. Kidd, G. Tan, X. Yin, R. Yang, Subambient cooling of water: toward real-world applications of daytime radiative cooling, Joule 3 (1) (2019) 111–123.

[11] X. Wang, X. Liu, Z. Li, H. Zhang, Z. Yang, H. Zhou, T. Fan, Scalable flexible hybrid membranes with photonic structures for daytime radiative cooling, Adv. Funct. Mater. 30 (5) (2020) 1907562.
[12] A. Leroy, B. Bhatia, C.C. Kelsall, A. Castillejo-Cuberos, L. Zhao, L. Zhang, A. Guzman, E. Wang, et al., High-performance subambient radiative cooling enabled by optically selective and thermally insulating polyethylene aerogel, Sci. Adv. 5 (10) (2019) eaat9480.
[13] Y. Peng, J. Chen, A.Y. Song, P.B. Catrysse, P.-C. Hsu, L. Cai, B. Liu, Y. Zhu, G. Zhou, D.S. Wu, et al., Nanoporous polyethylene microfibres for large-scale radiative cooling fabric, Nat. Sustain. 1 (2) (2018) 105–112.
[14] M. Yang, W. Zou, J. Guo, Z. Qian, H. Luo, S. Yang, N. Zhao, L. Pattelli, J. Xu, D.S. Wiersma, Bioinspired "skin" with cooperative thermo-optical effect for daytime radiative cooling, ACS Appl. Mater. Interfaces 12 (22) (2020) 25286–25293.
[15] Z. Chen, L. Zhu, A. Raman, S. Fan, Radiative cooling to deep sub-freezing temperatures through a 24-h day–night cycle, Nature Commun. 7 (1) (2016) 1–5.
[16] L. Zhu, A.P. Raman, S. Fan, Radiative cooling of solar absorbers using a visibly transparent photonic crystal thermal blackbody, Proc. Natl. Acad. Sci. 112 (40) (2015) 12282–12287.
[17] L. Zhu, A. Raman, K.X. Wang, M. Abo Anoma, S. Fan, Radiative cooling of solar cells, Optica 1 (1) (2014) 32–38.
[18] L. Zhu, A. Raman, S. Fan, Color-preserving daytime radiative cooling, Appl. Phys. Lett. 103 (22) (2013) 223902.
[19] A. Harrison, M. Walton, Radiative cooling of TiO2 white paint, Sol. Energy 20 (2) (1978) 185–188.
[20] L. Cai, Y. Peng, J. Xu, C. Zhou, C. Zhou, P. Wu, D. Lin, S. Fan, Y. Cui, Temperature regulation in colored infrared-transparent polyethylene textiles, Joule 3 (6) (2019) 1478–1486.
[21] S.N. Bathgate, S.G. Bosi, A robust convection cover material for selective radiative cooling applications, Sol. Energy Mater. Sol. Cells 95 (10) (2011) 2778–2785.
[22] Z. Chen, L. Zhu, W. Li, S. Fan, Simultaneously and synergistically harvest energy from the sun and outer space, Joule 3 (1) (2019) 101–110.
[23] M. Benlattar, E. Oualim, T. Mouhib, M. Harmouchi, A. Mouhsen, A. Belafhal, Thin cadmium sulphide film for radiative cooling application, Opt. Commun. 267 (1) (2006) 65–68.
[24] R. Zhu, D. Hu, Z. Chen, X. Xu, Y. Zou, L. Wang, Y. Gu, Plasmon-enhanced infrared emission approaching the theoretical limit of radiative cooling ability, Nano Lett. 20 (10) (2020) 6974–6980.
[25] Y. Chen, J. Mandal, W. Li, A. Smith-Washington, C.-C. Tsai, W. Huang, S. Shrestha, N. Yu, R.P. Han, A. Cao, et al., Colored and paintable bilayer coatings with high solar-infrared reflectance for efficient cooling, Sci. Adv. 6 (17) (2020) eaaz5413.
[26] Z.M. Zhang, Nano/Microscale Heat Transfer, Springer, 2007.
[27] A. Berk, G.P. Anderson, L.S. Bernstein, P.K. Acharya, H. Dothe, M.W. Matthew, S.M. Adler-Golden, J.H. Chetwynd, S.C. Richtsmeier, B. Pukall, et al., Modtran4 radiative transfer modeling for atmospheric correction, in: Optical Spectroscopic Techniques and Instrumentation for Atmospheric and Space Research III, Vol. 3756, International Society for Optics and Photonics, 1999, pp. 348–354.
[28] J.-l. Kou, Z. Jurado, Z. Chen, S. Fan, A.J. Minnich, Daytime radiative cooling using near-black infrared emitters, Acs Photon. 4 (3) (2017) 626–630.